Research Article

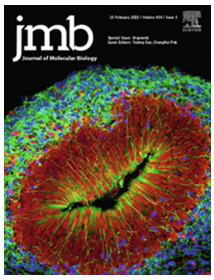

Protection of the Prodomain α1-Helix Correlates with Latency in the Transforming Growth Factor-β Family

Viet Q. Le [1], Roxana E. Iacob [2], Bo Zhao [1,3], Yang Su [1], Yuan Tian [1], Cameron Toohey [1], John R. Engen [2] and Timothy A. Springer [1]*

*1 - **Program in Cellular and Molecular Medicine,** Boston Children's Hospital and Department of Biological Chemistry and Molecular Pharmacology, Harvard Medical School, Boston, MA, United States*
*2 - **Department of Chemistry and Chemical Biology,** Northeastern University, Boston, MA, United States*
*3 - **Department of Immunology,** Molecular Cancer Research Center, School of Medicine, Sun Yat-sen University, Shenzhen, China*

***Correspondence to Timothy A. Springer:** springer@crystal.harvard.edu (T.A. Springer), @jrengen (J.R. Engen), @timothyspringer, @TimSpringerLab (T.A. Springer)*
https://doi.org/10.1016/j.jmb.2021.167439
Edited by Patrick Griffin

Abstract

The 33 members of the transforming growth factor beta (TGF-β) family are fundamentally important for organismal development and homeostasis. Family members are synthesized and secreted as pro-complexes of non-covalently associated prodomains and growth factors (GF). Pro-complexes from a subset of family members are latent and require activation steps to release the GF for signaling. Why some members are latent while others are non-latent is incompletely understood, particularly because of large family diversity. Here, we have examined representative family members in negative stain electron microscopy (nsEM) and hydrogen deuterium exchange (HDX) to identify features that differentiate latent from non-latent members. nsEM showed three overall pro-complex conformations that differed in prodomain arm domain orientation relative to the bound growth factor. Two cross-armed members, TGF-β1 and TGF-β2, were each latent. However, among V-armed members, GDF8 was latent whereas ActA was not. All open-armed members, BMP7, BMP9, and BMP10, were non-latent. Family members exhibited remarkably varying HDX patterns, consistent with large prodomain sequence divergence. A strong correlation emerged between latency and protection of the prodomain α1-helix from exchange. Furthermore, latency and protection from exchange correlated structurally with increased α1-helix buried surface area, hydrogen bonds, and cation-pi bonds. Moreover, a specific pattern of conserved basic and hydrophobic residues in the α1-helix and aromatic residues in the interacting fastener were found only in latent members. Thus, this first comparative survey of TGF-β family members reveals not only diversity in conformation and dynamics but also unique features that distinguish latent members.

Introduction

The TGF-β family comprises 33 genes that encode TGF-βs, bone morphogenetic proteins (BMPs), growth and differentiation factors (GDFs), and activins/inhibins. Family members regulate homeostasis, establish the anterior-posterior, ventral-dorsal, and left–right axes during embryonic development, and direct fine details of skeleton and organ development.[1,2] In general, members are synthesized as a proprotein composed of a large, divergent N-terminal prodomain and a smaller, more conserved C-terminal growth factor (GF) domain, separated by a proprotein con-

vertase (PC)/furin cleavage site. Prodomains are required for growth factor domain folding and dimerization,[3–5] storage in the extracellular matrix (ECM) or on cell surfaces,[6–16] and regulate growth factor activity and signaling range.[16–23]

Subsequent to disulfide bond formation and dimerization in the ER, family members are cleaved by PC/furin, usually in the Golgi, and secreted as pro-complexes of noncovalently associated prodomains and growth factor dimers. Pro-complexes of most members are active, i.e., non-latent, in that receptors can competitively displace the prodomains and bind the growth factor to initiate downstream signaling. In contrast, pro-complexes of other family members are latent,[24–33] including TGF-βs 1–3, GDF8 and its close relative GDF11, and GDF9 in some species and not others.[31] In these family members, prodomain association precludes receptor binding to the growth factor. Activation of latent TGF-βs 1 and 3 is mediated by integrins αVβ6 and αVβ8, which bind to an RGDLXX(L/I) motif in the prodomain arm domain[34–36], whereas activation of GDF8 and GDF11 is mediated by cleavage of the prodomain in the α2-helix by Tolloid (TLD) metalloproteases.[32,37]

The overall factors that regulate latency in the TGF-β family are incompletely understood. Structural studies of pro-complexes, including crystallography, nsEM, and hydrogen–deuterium exchange mass spectrometry (HDX-MS), have been confined to individual family members such as GDF8,[38,39] TGF-β1[36,40] and ActA,[41] or to close homologs like BMP7 and BMP9.[22,42] Broad comparative studies to determine whether unique structural or HDX signatures are predictive of latency have not been done. Here, we characterize a diverse set of latent and non-latent TGF-β family members using nsEM- and HDX-MS. First, we wanted to obtain an overview of differences and similarities among a diverse set of family members that included members of the TGF-β, activin, GDF, and BMP subfamilies. Second, we determined whether there were any unique features that could discriminate between latency and non-latency.

Results

Three overall pro-complex conformations

Using nsEM, we characterized conformations of latent TGF-β2 and non-latent BMP10 pro-complex dimers and compared them to previously published nsEM structures (Figure 1(A)–(F) and Supplemental Figure S1). TGF-β family prodomains consist of two portions: an N-terminal straitjacket that surrounds and packs against the growth factor, and a C-terminal arm domain that has a β-sandwich fold. TGF-β2 adopted a ring-like, cross-armed conformation similar to TGF-β1[40] (Figure 1(A) and (C)). BMP10 predominately adopted a nearly linear, open-armed conformation similar to its closest homolog, BMP9, and was also similar to BMP7[22] (Figure 1(B), (D), and (F)). Latent GDF8 displayed a V-shaped, V-armed conformation (Figure 1(E)) with its arm domains intermediate in orientation between the cross-armed conformation of the two TGF-βs and the open-armed conformation of the three BMPs.[38]

Crystal structures of TGF-β family members,[22,39–41] superimposed on their growth factor domains, are shown for comparison (Figure 1(G)–(J)). The cross-armed conformation of TGF-β2 and β1 matches the crystal structure of TGF-β1 (Figure 1(A), (C), and (G)), in which the arm domains of each prodomain monomer are disulfide linked to one another at their tips distal from the GF domains. On the opposite side of the ring from the arm and bowtie, the latency lasso and α1-helix wrap around the growth factor dimer to form the other half of the ring. The open-armed conformations of the three BMPs resemble the BMP9 crystal structure, in which the arm domains are oriented with their tips pointing away from one another (Figure 1(B), (D), (F), and (H)). The V-armed particles of latent GDF8 in nsEM correlate well with the crystal structure of latent GDF8[39] (Figure 1(E) and (I)). The crystal structure of BMP9 has a more open V-shape than GDF8, which in turn is more open than the V of ActA (Figure 1(H)–(J)). Heterogeneity among BMP class averages in V-angle (Figure 1(B), (D) and (F)) and the presence of an S-shape (Figure 1(D)) may reflect genuine conformational flexibility and also effects of adsorption onto the EM grid.

TGF-β family pro-complexes exhibit disparate patterns of HDX overall

Next, we measured HDX of TGF-β1, TGF-β2, BMP7, BMP9, BMP10, and ActA at pH 7.5 and include published HDX data for GDF8[38] at pH 7.5 for comparison. We obtained 73–90% sequence coverage overall (Table S1) with nearly 100% coverage of the prodomains (Figure 2, Supplemental Figures S2–S9). In contrast, coverage in the disulfide-rich growth factor domains was lower (and depressed the overall coverage percent) due to incomplete reduction of the disulfide bonds in the HDX quench conditions and poorer pepsin digestion. HDX for the eight TGF-β family members was measured at 5–6 time points spanning a broad time range of 10-s to 4-h (see Table S1, Figures S2–S9, and raw data in PRIDE ID PXD026841). Our interpretation and discussion will focus mainly on the 1-min and 60-min time points (Figure 2) for single peptides that maximally tile the sequences of family members that are aligned by sequence and structure. As different protein regions exchange with different rates, the 1- and 60-min timepoints provide snapshots of exchange during the wide range of timepoints measured. Biological assays of TGF-β latency require just a single event of growth factor release from the prodomain and have multi-hour timescales. All comparisons of backbone

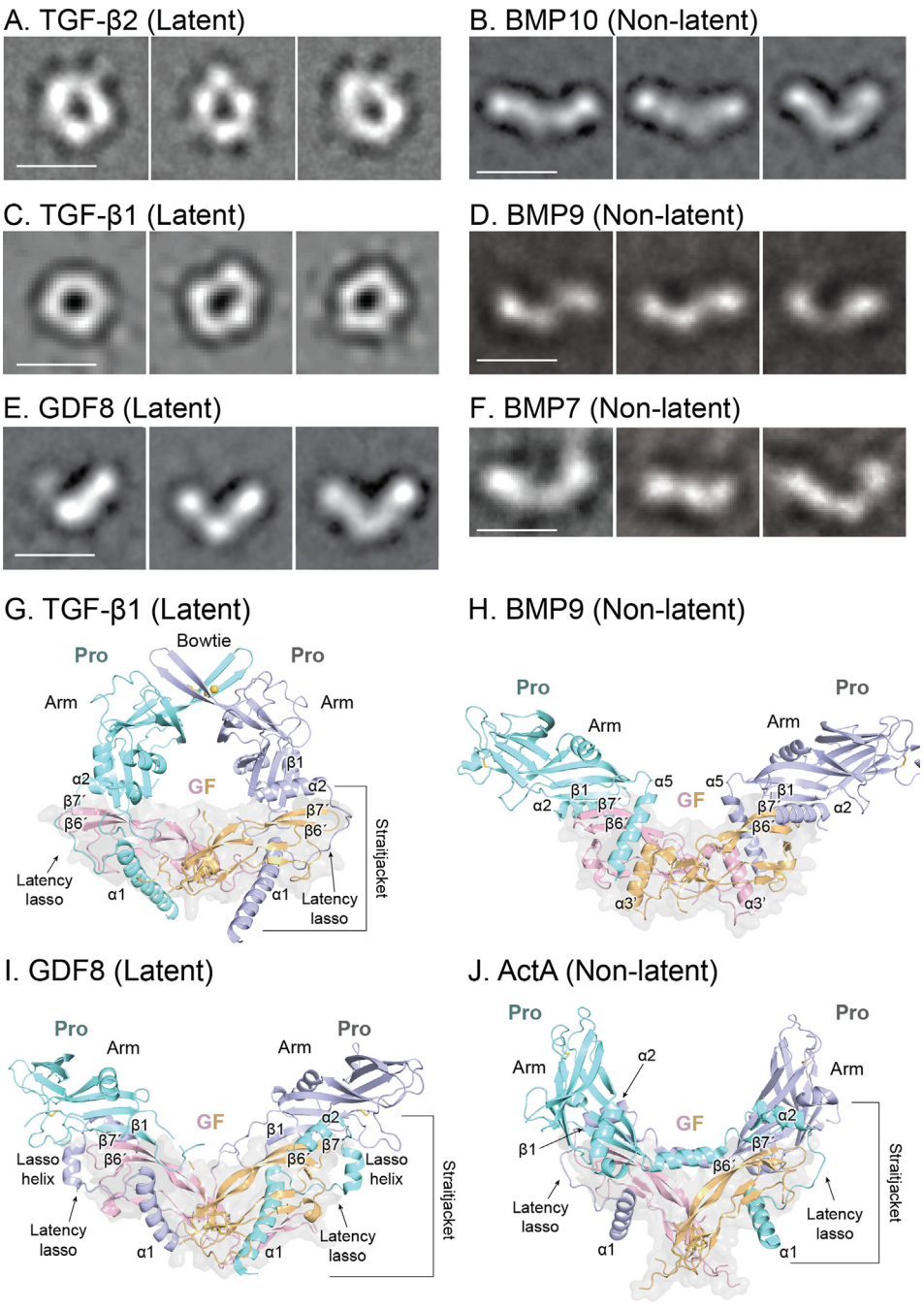

Figure 1. Structure and conformation of TGF-β family member pro-complexes. (A–F) Representative negative stain EM class averages of TGF-β2 and BMP10 compared to previously published class averages of TGF-β1, BMP9, GDF8, and BMP7.[22,38,40] Scale bars = 10 nm. (G–J) Crystal structures of TGF-β1, BMP9, GDF8, and ActA superimposed on their GF dimers.[22,39,41,50] Yellow spheres indicate the position of the bowtie disulfide bonds in TGF-β1 (G). The solvent accessible surface of the GF is shown as a transparent gray surface. Pro = prodomain. GF = growth factor.

amide HDX between TGF-β family members are qualitative because our HDX-MS measurements were of relative deuterium incorporation and were not corrected for back-exchange during analysis (despite best efforts, maximally deuterated controls could not be reliably prepared for these proteins). As nsEM showed that TGF-β2 had a structure similar to TGF-β1, and BMP7 and BMP10 had structures similar to BMP9, the alignments in Figure 2 were used to display the HDX after one minute on the corresponding crystal structures in Figure 3.

HDX of proteins with identical overall folds can be compared[43–45], provided the interpretation remains mostly qualitative, as has been successfully done

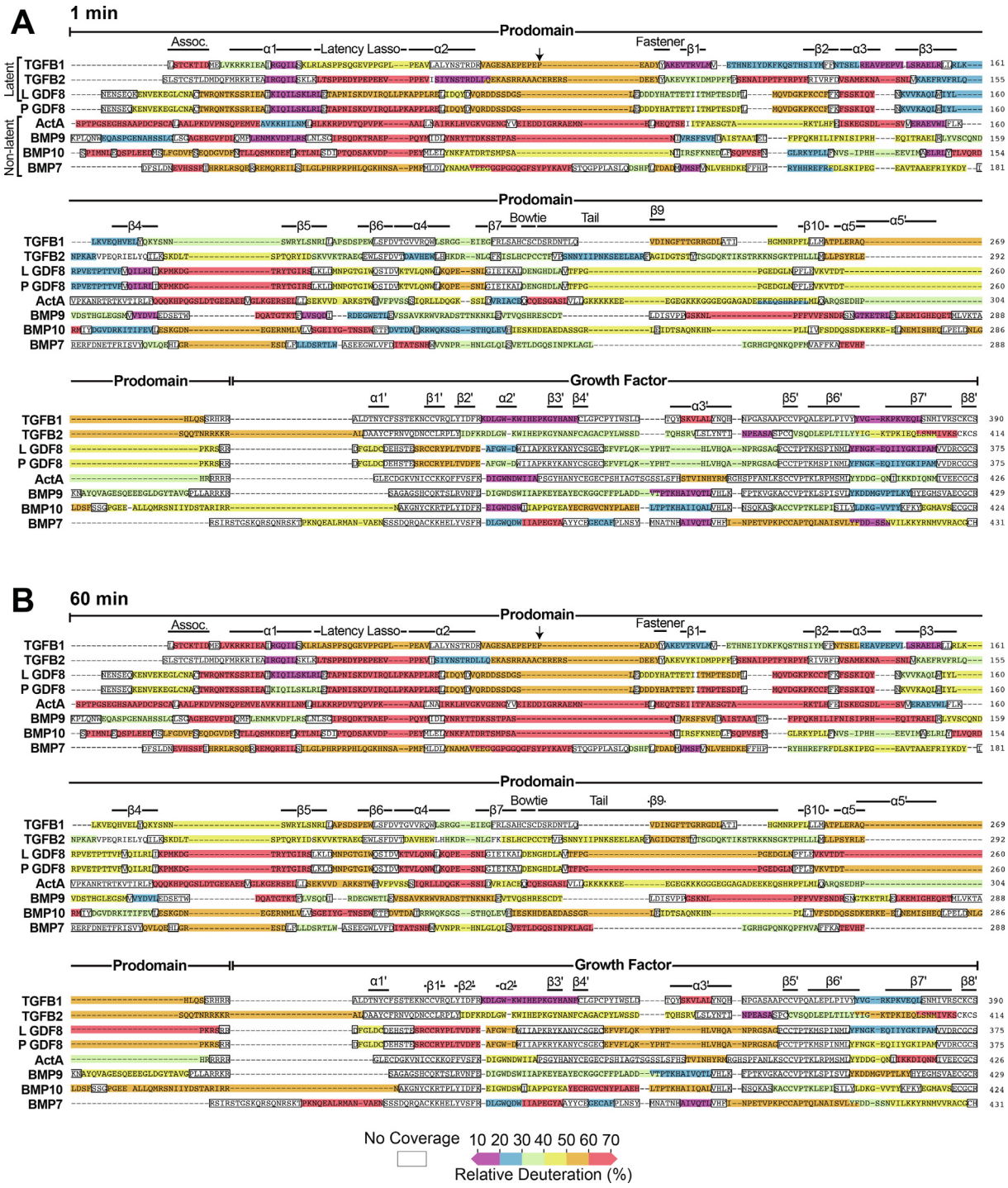

Figure 2. Hydrogen-deuterium exchange of TGF-β family members indicated on their sequences. (A and B) Deuteration at 1 min (*A*) and 60 min (*B*). Select peptides from each complete dataset (shown in Supplemental Figures S2–S9) were chosen to maximize sequence coverage without overlapping, with considerations made for peptides of similar length and alignment to conserved structural features to allow comparisons between family members. Relative deuteration of each peptide is indicated by color according to the key shown. The data are overlaid onto a sequence alignment of all proteins investigated that has been corrected to align structurally homologous positions. Prodomain and growth factor boundaries and structural elements are marked above the alignment. Dashes represent gaps in the sequence alignment and are colored if sequences at each end are included in a peptide covered by HDX-MS. Regions that lack HDX peptide coverage or correspond to the rapidly back-exchanging N-terminal residue of peptides are shown as unfilled rectangles. A downward arrow indicates the position of the Cys residue found in the α2-fastener loop of TGF-β2 but not of TGF-β1.

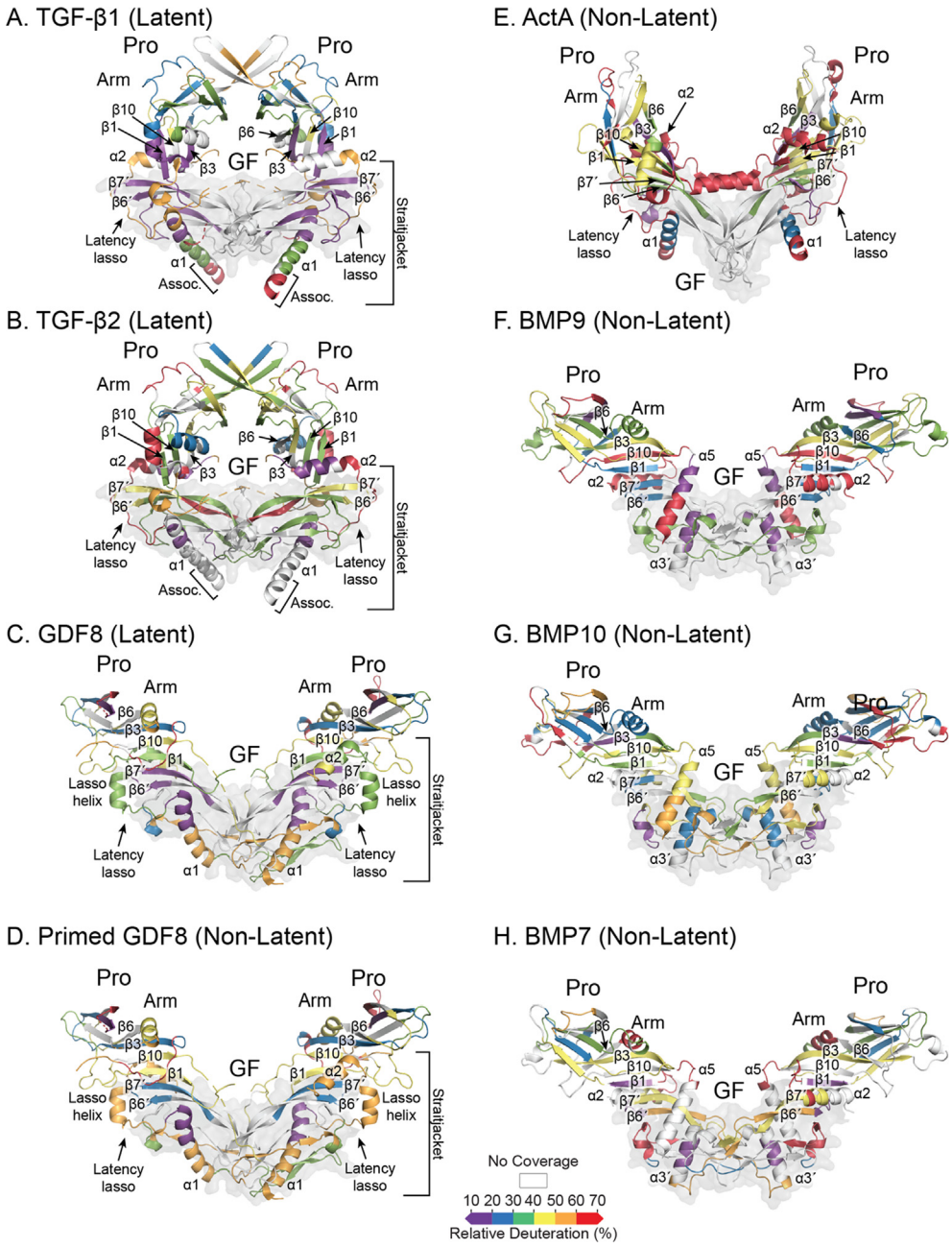

Figure 3. Hydrogen-deuterium exchange of TGF-β family members indicated on structures. (A–H) Deuterium exchange at 1 min is colored onto ribbon diagrams of crystal structures or onto crystal structures of the closest homologue using the same peptides and alignments shown in Figure 2. TGF-β2 utilizes the TGF-β1 crystal structure and BMP7 and BMP10 utilize the BMP9 crystal structure. In panel *D*, data for primed GDF8 is displayed on the structure of latent GDF8. The GF is shown as a gray transparent surface as in Figure 1. HDX-MS data for all time points are found in Supplemental Figures S2-S9.

previously for many systems including GDF8:TGF-β1,[38] integrins,[46] heme-oxygenases,[47] Ras-family proteins,[45] processivity clamps,[43] and allelic variants of HIV Nef.[44] Thus, our HDX comparisons between TGF-β family members focus on structural elements of the prodomains and growth factors that are well-conserved in the family despite differences in overall pro-complex conformation and sequence.[48]

Strikingly, overall exchange varied greatly even among the most closely related members studied here. Due to protein dynamics, intrinsic exchange was higher almost everywhere in TGF-β2 than β1 (Figures 2 and 3(A) and (B)). Additionally,

differences were also pronounced among BMP7, 9, and 10 (Figures 2 and 3(F)–(H)). These differences were consistent with the large sequence variation among prodomains. For example, among closely related family members, the TGF-β1 and β2 GFs are 71% identical while their prodomains are 39% identical; the BMP9 and BMP10 GFs are 64% identical while their prodomains are only 33% identical. As dissociation of the prodomain from the GF is required for Type 1 and Type 2 receptor binding, this remarkable variability in exchange suggests variation in regions of the prodomain that are most susceptible to breathing movements (fast exchange) with important implications for GF dissociation, i.e., activation.

Variability in exchange among family members was evident throughout their prodomains. The first portion of the prodomain is called the association region because in TGF-β1, β2, and β3 it contains the conserved Cys residue that disulfide links to a milieu molecule that mediates pro-complex storage in either the ECM or on cell surfaces.[12,13,15,16,48] The complex crystal structure of TGF-β1 linked to the milieu molecule glycoprotein A repetitions predominant (GARP) shows that each TGF-β1 monomer forms a buried interface with GARP that involves varying lengths of amino acid residues flanking the conserved Cys, e.g., ^{30}-LSTCKTID-^{37} in one monomer and ^{32}-TCKTI-^{36} in the other.[49] The longer 8-residue sequence was used to define the association region in Figures 2 and 3. No milieu molecules were present in our study, and in the absence of a partner, the association region of TGF-β1 was highly deuterated even after one minute. Unlike TGF-β1, peptides corresponding to the association region of TGF-β2 were not covered in HDX. The N-terminal segment containing the association region is often longer in other family members and is unstructured in GDF8, ActA, and BMP9 crystal structures[22,39,41] which have no known milieu molecules that associate in this region. The N-terminal peptides in other family members exhibited high HDX even at the shortest time points (Figures S2–S9), except for BMP9 which exchanged less throughout the time course (Figures 2 and S2–S9).

The α1-helix immediately following the association region also differed in exchange between family members. In TGF-β1, TGF-β2, and latent GDF8, peptides from the C-terminal half of the α1-helix were strongly protected from exchange. In contrast, similar α1-helix peptides from the activated form of GDF8 (primed GDF8), ActA, and the three BMPs exhibited moderate-to-high exchange at the 60-min time point (Figures 2 (B) and S4–S6). In crystal structures of TGF-β1, ActA, and GDF8 pro-complexes, the α1-helix adopts a similar conformation (Figure 3); the lower HDX of TGF-β1 and GDF8 than ActA are consistent with greater burial and number of polar noncovalent bonds as described in Discussion. In contrast, in BMP9 pro-complex crystal structures no density is apparent for the α1-helix; the α5-helix appears in a similar location but with a distinct orientation.

The correlation between low exchange of the prodomain α1-helix and latency is illustrated in more detail for the three latent members and one non-latent counterexample in Figure 4**.** The C-terminal half of the α1-helix in latent TGF-β1, TGF-β2, and GDF8 was highly protected from exchange (Figure 2(B), peptide 1 in Figure 4(A)–(C)). However, this region of the α1-helix in non-latent Activin A, BMPs 7, 9, and 10, and primed GDF8 exchanged more rapidly (Figure 2(B), peptide 1 in Figure 4(C) and (D)). Figure 4 shows an important interface between the prodomain and growth factor, including the prodomain β1 strand that hydrogen bonds to the growth factor finger containing the β6′ and β7′ strands, and the prodomain α1-helix, latency lasso, and α2-helix that pack against and surround the growth factor finger containing the β6′ and β7′ strands. Nonetheless, plots of the kinetics of exchange for these regions show that the only element with a strong correlation to latency is the C-terminal portion of the α1-helix.

The straitjacket encircles the growth factor domain in structures of TGF-β1, GDF8, and ActA (Figure 3(A)–(E)). The straitjacket consists of the α1-helix, the latency lasso, which is a highly deuterated loop (Figures 2 and 3(A)–(E)), and the α2-helix, which forms a conserved interface with the convex surface of the growth factor domain on the side opposite to the cleft inhabited by the prodomain α1-helix (Figure 3). Low exchange of the α2-helix was only apparent in TGF-β2, although peptides corresponding to the α2-helix in TGF-β1 were not covered.

HDX differences extend into the prodomain arm domain, which contains two conserved 4-stranded antiparallel β-sheets (Figure 3).[22,39–41,50] Regions of differences included the β1-strand, which initiates the arm domain, and the β3-strand (Figure 2(B)).

HDX differences were also found in the growth factor domains, particularly the α3′ helix and the β6′-β7′ strand regions. In BMP9, the α3′ helix is well formed, whereas it is disordered in GDF8 and ActA, correlating with the observed low and high levels of deuteration, respectively, in the α3′ helix (Figure 2(B)). Low exchange was observed in the C-terminal end of the β6′ strand and the N-terminal half of the β7′ strand of TGF-β1 and latent GDF8, whereas higher exchange was observed for this region in the remaining family members including, notably, TGF-β2 (Figures 2 and 3).

Discussion

Our nsEM and HDX-MS studies presented here offer important insights into the diversity of pro-

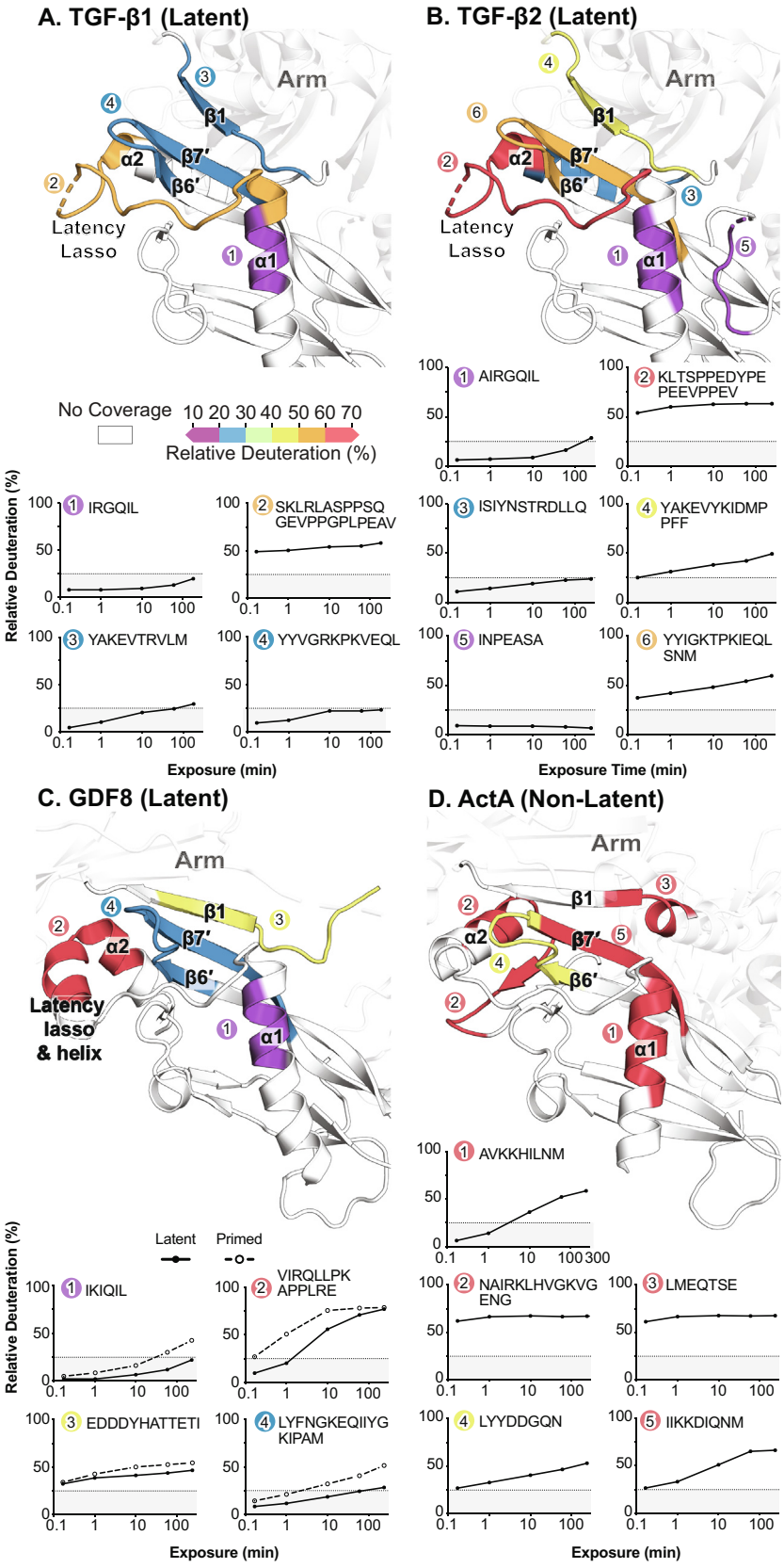

Figure 4. HDX in straitjacket–growth factor interfaces. (A–D) Interfaces are shown for the indicated family members. In the top half of each panel, peptides are colored according to exchange after 1 h, using the key shown. In the bottom half of each panel, HDX uptake graphs are shown for the same select peptides keyed by number and color. Gray boxes indicate percent deuteration in the 0–25% range. HDX data for latent and Tolloid-cleaved GDF8 are plotted as solid and dashed lines, respectively.

complex structures and show that among many measures, only α1-helix exchange kinetics correlates with latency among the three latent and five non-latent TGF-β family members studied. Extension of nsEM studies to TGF-β2 and BMP10 pro-complexes, which were previously uncharacterized structurally, revealed a cross-armed conformation for TGF-β2 and an open-armed conformation for BMP10. Together with our previous nsEM work, these results further highlight the existence of at least three pro-complex conformational states: cross-armed, open-armed, and V-armed. Cross-armed pro-complexes have thus far only been found to be latent, i.e., TGF-β1 and β2, whereas V-armed pro-complexes can be either latent (GDF8) or non-latent (ActA). Meanwhile, open-armed conformations have only been found to be non-latent as illustrated by BMP7, 9, and 10.

Importantly, our comparative HDX studies on multiple family members revealed that low exchange in the C-terminal portion of the prodomain α1-helix correlated strongly with latency. Latent TGF-β1, TGF-β2, and GDF8 showed low exchange in this region with less than 25% exchange by 4 h whereas non-latent ActA, BMP7, BMP9, and BMP10 all showed moderate-to-high exchange in the same timeframe. The α1-helix is a key region of the prodomain that interacts with the GF, and low HDX in both the prodomain α1-helix and GF β6′–β7′ region of TGF-β1 and GDF8 suggest that these elements form a stable interface that contributes to strong prodomain–growth factor binding. Meanwhile, the greater exchange of the GF β6′–β7′ region in TGF-β2 compared to TGF-β1 suggests a less stable interface with the α1-helix and that different structural features among latent members impinge on the α1-helix to help maintain latency. Overall, our studies strongly suggest that a protected, less dynamic prodomain α1-helix occupying the GF hydrophobic cleft is a signature feature of latency. This is especially remarkable because different structural elements are involved in release from latency. GDF8 and its sister GDF11 are activated by cleavage in the α2-helix near the α1-helix in the straitjacket. In contrast, binding of integrins αVβ6 and αVβ8 to a motif in the shoulder of the arm domain, distal from the α1-helix, activates TGF-β1 and TGF-β3.

Among latent members studied, TGF-β2 is not only distinguished by greater exchange in the GF β6′–β7′ region but is also more dynamic/deuterated overall. Compared to TGF-β1, TGF-β2 has a much longer prodomain with 283 residues compared to 249 in TGF-β1 and many insertions and deletions (Figure 2). Larger size may offset the faster dynamics of the prodomain by stabilizing it[51] and thus contribute to latency. Several candidate regions also emerge that may also contribute to TGF-β2 latency. The first is low exchange in the C-terminal portion of the prodomain α2-helix in the TGF-β2 straitjacket (Figure 2). In structures of latent TGF-β1 and GDF8, the α2-helix nestles against the convex side of the GF β6′-β7′ region (Figure 4(A) and (C)). Although the corresponding peptide was not observed in HDX for TGF-β1, this region in latent GDF8 and all non-latent members is more deuterated suggesting a key difference in the α2-helix of TGF-β2. Secondly, a peptide (INPEASA) mapping to the α3′-β5′ loop exhibits low exchange in TGF-β2 (Figure 2). Although the corresponding peptide was not recovered in TGF-β1, in TGF-β1 structures the corresponding peptide forms varying H-bond networks with the sidechains of Arg-45 and Gln-52 in the α1-helix (Figure 5(C)) and thus could interact with and stabilize the α1-helix. Furthermore, a Cys residue is present between the α2-helix and the fastener in TGF-β2 but not in TGF-β1 (arrow in Figure 2). This Cys residue likely disulfide links to its partner in the other prodomain. The fastener forms important interactions with the α1-helix and completes the encirclement of the growth factor β6′-β7′ finger by the straitjacket. Disulfide linkage between the straitjackets in each monomer would cooperatively stabilize them.

We further examined crystal structures of TGF-β family members for structural correlates of lower exchange of the prodomain α1-helix in latency. Buried solvent accessible surface area correlates well with stability of interactions between proteins; therefore, we calculated burial for α1-helix and fastener residues (overlined in Figure 5(A)). The buried solvent accessible surface areas for the α1-helix and fastener of TGF-β1 and GDF8 were similar and were each substantially greater compared to ActA (Figure 5(B)). The number of hydrogen bond and cation-pi interactions that the α1-helix made with the growth factor or prodomain were also greater for latent TGF-β1 and GDF8 structures than for ActA (Figure 5(C)–(E)). All hydrogen bond and cation-pi interactions were found in the C-terminal portion of the α1-helix where HDX was low, from Arg-45 to Arg-58 in TGF-β1 and from Arg-52 to Arg-65 in GDF8 (Figure 5(A), (C) and (D)). The prodomain fastener, an excursion in the loop between the α2-helix and β1-strand toward the α1-helix, makes many of the important stabilizing interactions with the α1-helix. These include cation-pi bonds and mainchain-mainchain hydrogen bonds that cap the α1-helix. These important interactions are present in latent TGF-β1 and GDF8 but not in non-latent ActA (Figure 5(C)–(E)).

Demonstration here that protection of the C-terminal end of the prodomain α1-helix from HDX correlates with latency suggests that exposure of this portion of the α1-helix may occur during release of the GF from latency. Previous studies have pointed to the importance of the α1-helix in latency. Mutation to alanine of hydrophobic

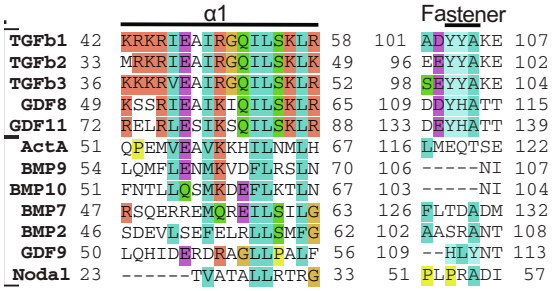

B.

Protein	PDB	N	Buried surface area, BSA	
			α1-helix	Fasten
TGF-β1 (Latent)	5vqp, 5vqf, 5ffo, 6gff	13	923±55	237±1
GDF8-1 (Latent)	5ntu	2	808±46	280±4
ActA (Non-Latent)	5hly, 5hlz	6	594±22	117±3

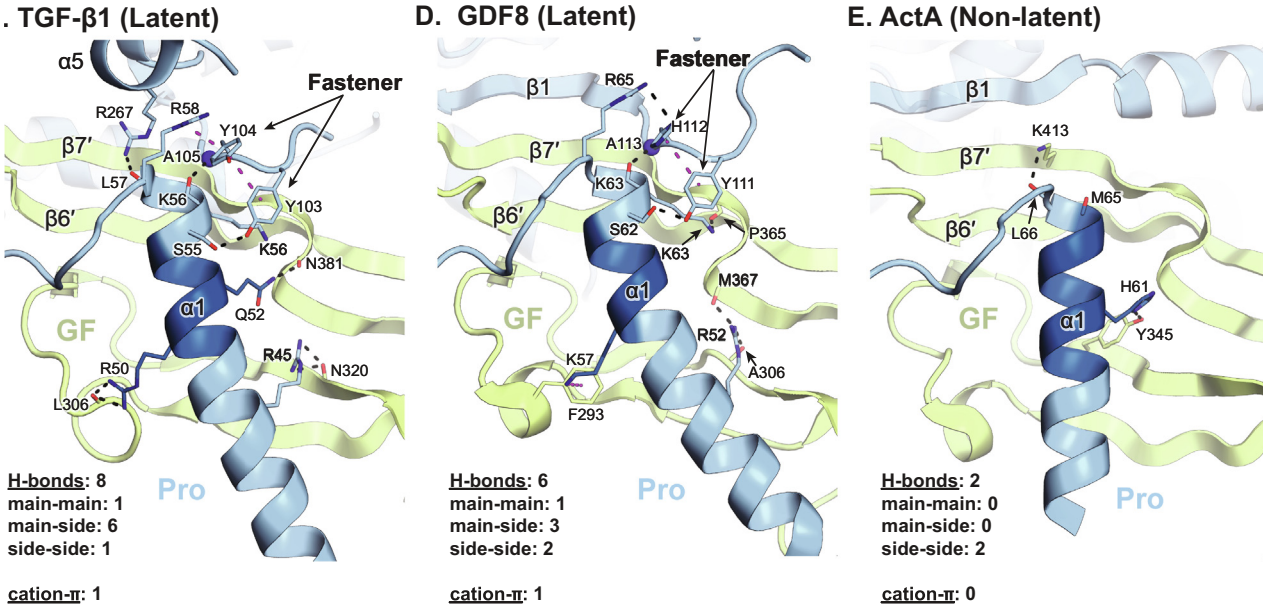

Figure 5. The α1-helix, fastener, and their interaction networks. (A) Sequence alignment of α1-helix and fastener regions of representative family members. Dark orange = basic. Teal = hydrophobic. Purple = acidic. Light orange = glycine. Green = uncharged polar. Yellow = proline. (B) Solvent accessible surface area buried on α1-helix and fastener residues overlined in panel A was calculated using the PISA server[69] including the GF monomer that is surrounded by the straitjacket, and omitting the other monomer, which was disordered in this region in some and not in other structures. For TGF-β1 and ActA, data are mean and s.d. of all independent monomeric units in the listed PDB accessions. For GDF8, data are mean and difference from the mean of each independent monomeric unit in the listed PDB accession. (C–E) Ribbon cartoons of the α1-helix and its environment in TGF-β1 (*C*, PDB code 5vqp, chains A and B), GDF8 (*D*, PDB code 5ntu, chains A and B), and ActA (*E*, PDB code 5hlz, chains A, B, and C). The prodomain (Pro) is shown in blue, the growth factor (GF) is shown in green. Hydrogen and pi bonds to the α1-helix as well as pi bonds within the fastener are shown as black and magenta dashes, respectively. The backbone amide of A105 (C) and A113 (D) are shown as blue spheres.

residues Ile-53, Leu-54, Leu-57, and Leu-59 and basic residues Arg-45, Arg-50, Lys-56, and Arg-58 in the α1-helix all led to increased release of the TGF-β1 growth factor.[52] Mapping studies of the minimum inhibitory prodomain fragment of GDF8 yielded fragments of varying lengths that all included the α1-helix[53–55]; medicinal chemistry efforts have obtained peptides that are full α1-helix-like and antagonize the growth factor with ~1 μM IC_{50} values.[56]

The fastener has also been shown to be important in latency. Mutation of TGF-β1 fastener residues Tyr-103 or Tyr-104 to Ala abolished latency.[40] A role for the fastener was further demonstrated by introduction of TGF-β1 fastener sequences into an ActA prodomain Fc fusion construct, which greatly enhanced its inhibition of ActA growth factor activity.[57] In GDF8, alanine mutations of equivalent fastener residues Tyr-111 and His-112 and of the α1-helix residue Arg-65, which forms an H-bond with His-112 (Figure 5(D)), increased basal activity over the wild type latent form.[39,58]

Sequence alignments revealed remarkably strong sequence conservation in the α1-helix of all

latent family members (TGF-β1–3, GDF8, and GDF11) with a consensus R(I/V/L)E(A/S)(R/K)I(R/K)XQILSKL(R/K) sequence (Figure 5(A)). In contrast, this region is much more divergent in non-latent family members (Figure 5(A)).[48] Moreover, the fastener regions of latent members are all characterized by conserved, adjacent tyrosine and histidine aromatic residues that can participate in pi-pi interactions with one another and with α1-helix basic residues in cation-pi interactions (Figure 5(A)).

Our nsEM and HDX-MS results point to rich diversity in the overall conformation, dynamics, and structural details (including prodomain–growth factor interfaces) in the TGF-β family. Moreover, structural dynamics investigation by HDX-MS has provided important context for interpreting existing crystal structures and insights into functional differences in the family. In particular, our HDX results coupled with strong sequence conservation of the α1-helix and fastener suggests that prodomain–GF association is sufficient for conferring latency only for TGF-β1–3 and GDF8 and 11, whereas latency in other family members may require association with a binding partner in the extracellular milieu.

Experimental Procedures

Protein expression and purification

Human TGF-β2 was cloned into the pEF-puro vector with N-terminal 8xHIS and streptavidin-binding peptide (SBP) purification tags,[40] a C24S mutation, an N140R mutation to remove one N-glycan site, and abolition of furin cleavage by replacing the residues 298–302 (RRKKR) with a glycine residue. This TGF-β2 construct was stably expressed in 293S GnTI$^{-/-}$ cells to produce protein with high-mannose glycosylation, purified by His and Streptactin affinity chromatographies, and dialyzed into 20 mM Tris-HCl pH 7.5, 500 mM NaCl with Precision3C protease to remove purification tags. Cleaved TGF-β2 was then purified by Superdex200 size-exclusion chromatography (SEC) in 20 mM Tris-HCl pH 7.5, 500 mM NaCl.

Full-length human Activin A (wild type) and full-length BMP10 carrying N67Q and N131Q N-glycosylation site mutations and replacement of residues 312–316 (ARIRR) with a glycine residue to abolish furin cleavage were cloned into the S2-2 vector (ExpreS2ion Biotechnologies) with N-terminal 8xHis and SBP tags and stably integrated into *Drosophila* S2 cells. Cells were adapted to growth in serum-free Excell 420 media. After 4 days, culture supernatant was collected, filtered, buffer exchanged to 20 mM Tris-HCl pH 7.5, 500 mM NaCl and loaded onto a Ni-NTA column (Qiagen). The column was washed with 20 mM Tris, pH 7.5, 500 mM NaCl and 20 mM imidazole, and protein was eluted with 20 mM Tris-HCl, pH 7.5, 500 mM NaCl, and 1 M imidazole. Pooled elution fractions were dialyzed into 20 mM Tris, pH 7.5, 500 mM NaCl and simultaneously cleaved with Precision3C to remove the His-SBP tag. Cleaved ActA and BMP10 protein samples were then dialyzed against 20 mM Tris-HCl pH 7.5, 150 mM NaCl and subjected to another round of Ni-NTA chromatography to remove uncleaved material. The flow-through was then loaded onto a Superdex 200 column equilibrated with 20 mM Tris-HCl pH 7.5, 150 mM NaCl for SEC.

Negative stain electron microscopy

Purified TGF-β2 and BMP10 were subjected to SEC in 20 mM Tris-HCl pH 7.5, 150 mM NaCl immediately prior to negative-stain EM analysis to remove any aggregates. The peak fractions were loaded onto glow-discharged carbon-coated grids, buffer was wicked off, and grids were immediately stained with 0.75% (wt/vol) uranyl formate and imaged with an FEI Tecnai T12 microscope and Gatan 4 K × 4 K CCD camera at 52,000× magnification (2.13 Å pixel size at specimen level) with a defocus of − 1.5 μm. Well-separated particles (>5000) were interactively picked using EMAN2.[59] Class averages were calculated by multireference alignment followed by K-means clustering using SPIDER.[38,60–62] Software applications were made available and supported by SBGrid.[63]

Hydrogen deuterium exchange mass spectrometry (HDX-MS)

HDX-MS studies were performed using methods reported previously.[38,64,65] Additional experimental details are provided in Table S1 per the recommended format.[66] ActA, BMP10, and TGF-β2 were expressed and purified in this study, whereas wild type human BMP7, a BMP9 chimera composed of the mouse prodomain and human growth factor domain, and human TGF-β1 carrying a C4S mutation, N-glycosylation site mutations N107Q and N147Q, and a R249A mutation to abolish furin cleavage were expressed and purified in other studies.[22,50] All HDX-MS experiments were performed with proteins buffer exchanged into 20 mM Tris-HCl, pH 7.5, 150 mM NaCl with the exception of BMP9, which was buffer exchanged into PBS (1.8 mM KH_2PO_4, 10 mM Na_2HPO_4, 137 mM NaCl), pH 7.4 (a difference of 0.1 pH unit compared to the other proteins, at pH 7.5, will not significantly affect the final HDX conclusions). Samples (3 μL) of ActA (120.4 μM), BMP7 (272 μM), BMP9 (17 μM), BMP10 (60 μM), TGF-β1 (30 μM), and TGF-β2 (29 μM) were individually diluted 15-fold into 20 mM Tris, 150 mM NaCl, 99% D_2O (pD 7.5) at room temperature for deuterium labeling. At time points ranging from 10 sec to 240 min, aliquots were removed and deuterium exchange was quenched by adjusting the pH to 2.5 with an equal volume of cold 150 mM potassium phosphate, 0.5 M tris (2-carboxyethyl) phosphine hydrochloride (TCEP-

HCl), H_2O. Quenched samples were digested online using a Poroszyme immobilized pepsin cartridge (2.1 mm × 30 mm, Applied Biosystems) at 15 °C for 30 s, then injected into a custom Waters nanoACQUITY UPLC HDX Manager™ for mass analysis with a XEVO G2 mass spectrometer (Waters Corp., USA). The average amount of back-exchange using this experimental setup was 30–35%, based on analysis of highly deuterated peptide standards. All comparison experiments were done under identical experimental conditions such that deuterium levels were not corrected for back-exchange and are therefore reported as relative.[67] The error of measuring the mass of each deuterated peptide averaged ± 0.15 Da across two technical replicates as given by the DynamX software, which in some cases is an average of more than one charge state.

Peptic peptides were identified from triplicate undeuterated samples using high definition collision-induced dissociation mass spectrometry ($HDMS^E$). Data were analyzed using ProteinLynx Global SERVER (PLGS) 3.0.1 (Waters Corporation). A database containing only the sequences from human INHBA (ActA; Uniprot P08476), human BMP7 (Uniprot P18075), human BMP10 (Uniprot O95393), mouse GDF2 (BMP9; Uniprot Q9WV56) residues 23–318, human GDF2 (BMP9; Uniprot Q9UK05) residues 320–429, human GDF8 (Uniprot O14793), human TGFB1 (Uniprot P01137), and human TGFB2 (Uniprot P61812) was used with no cleavage specificity and no PTMs considered. Peptide masses were identified using a minimum of 130 ion counts for low energy threshold and a 50-ion count threshold for their fragment ions. The peptides identified in PLGS were then analyzed in DynamX 3.0 (Waters Corporation) implementing a minimum products per amino acid cut-off of 0.2, 2 consecutive product ions, and a maximum MH^+ error of 10 ppm. Those peptides meeting the filtering criteria were further processed by DynamX to calculate relative % deuteration and display it on the sequence and tertiary structure. No subtractive methods were used for overlapping peptides; all peptides including overlapping are shown in Supplemental Figures S2–S9, and when mapped to a crystal structure (Figures 3 and 4) only representative peptides were used without subtractive manipulation.

Data availability

All HDX-MS data have been deposited to the ProteomeXchange Consortium via the PRIDE[68] partner repository with the dataset identifier PXD026841.

CRediT authorship contribution statement

Viet Q. Le: Conceptualization, Methodology, Formal analysis, Investigation, Data curation, Writing – original draft, Visualization, Funding acquisition. **Roxana E. Iacob:** Methodology, Formal analysis, Validation, Investigation, Writing – review & editing. **Bo Zhao:** Methodology, Investigation, Writing – review & editing. **Yang Su:** Software, Writing – review & editing, Visualization. **Yuan Tian:** Methodology, Investigation, Writing – review & editing, Funding acquisition. **Cameron Toohey:** Investigation. **John R. Engen:** Resources, Writing – review & editing, Project administration, Funding acquisition. **Timothy A. Springer:** Conceptualization, Writing – review & editing, Supervision, Project administration, Funding acquisition.

Acknowledgement

The authors would like to thank Melissa Chambers and Zongli Li for help with EM data collection, Jordan Anderson for critical discussions, and Margaret Nielsen for her assistance in designing figures. We acknowledge a research collaboration with the Waters Corporation (J.R.E.).

Funding and additional information

This work was supported by NIH Grants R01-CA210920 and R01-AR067288 (T.A.S.). V.Q.L. was supported by NIH 5T32DK007527-35. Y.T. was supported by a Komen postdoctoral research fellowship (Komen PDF15334161).

Declaration of Competing Interest

The authors declare that they have no known competing financial interests or personal relationships that could have appeared to influence the work reported in this paper.

Appendix A. Supplementary data

Supplementary data to this article can be found online at https://doi.org/10.1016/j.jmb.2021.167439.

Received 22 September 2021;
Accepted 29 December 2021;
Available online 4 January 2022

Keywords:
activin;
bone morphogenetic protein (BMP);
electron microscopy (EM);
hydrogen exchange mass spectrometry;
transforming growth factor beta (TGF-β)

References

1. Wu, M.Y., Hill, C.S., (2009). TGF-β superfamily signaling in embryonic development and homeostasis. *Dev. Cell* **16**, 329–343.

2. Weiss, A., Attisano, L., (2013). The TGFβ superfamily signaling pathway. *Wiley Interdiscip. Rev. Dev. Biol.* **2**, 47–63.
3. Gray, A.M., Mason, A.J., (1990). Requirement for activin A and transforming growth factor–β1 pro-regions in homodimer assembly. *Science* **247**, 1328–1330.
4. Sha, X., Yang, L., Gentry, L.E., (1991). Identification and analysis of discrete functional domains in the pro region of pre-pro-transforming growth factor beta 1. *J. Cell Biol.* **114**, 827–839.
5. Neugebauer, J.M., Kwon, S., Kim, H.S., Donley, N., Tilak, A., Sopory, S., et al., (2015). The prodomain of BMP4 is necessary and sufficient to generate stable BMP4/7 heterodimers with enhanced bioactivity in vivo. *Proc. Natl. Acad. Sci. USA* **112**, E2307–E2316.
6. Miyazono, K., Hellman, U., Wernstedt, C., Heldin, C.H., (1988). Latent high molecular weight complex of transforming growth factor β1. Purification from human platelets and structural characterization. *J. Biol. Chem.* **263**, 6407–6415.
7. Saharinen, J., Keski-Oja, J., (2000). Specific sequence motif of 8-Cys repeats of TGF-β binding proteins, LTBPs, creates a hydrophobic interaction surface for binding of small latent TGF-β. *Mol. Biol. Cell* **11**, 2691–2704.
8. Gregory, K.E., Ono, R.N., Charbonneau, N.L., Kuo, C.L., Keene, D.R., Bachinger, H.P., et al., (2005). The prodomain of BMP-7 targets the BMP-7 complex to the extracellular matrix. *J. Biol. Chem.* **280**, 27970–27980.
9. Sengle, G., Charbonneau, N.L., Ono, R.N., Sasaki, T., Alvarez, J., Keene, D.R., et al., (2008). Targeting of bone morphogenetic protein growth factor complexes to fibrillin. *J. Biol. Chem.* **283**, 13874–13888.
10. Li, S., Shimono, C., Norioka, N., Nakano, I., Okubo, T., Yagi, Y., et al., (2010). Activin A binds to perlecan through its pro-region that has heparin/heparan sulfate binding activity. *J. Biol. Chem.* **285**, 36645–36655.
11. Anderson, S.B., Goldberg, A.L., Whitman, M., (2008). Identification of a novel pool of extracellular pro-myostatin in skeletal muscle. *J. Biol. Chem.* **283**, 7027–7035.
12. Stockis, J., Colau, D., Coulie, P.G., Lucas, S., (2009). Membrane protein GARP is a receptor for latent TGF-β on the surface of activated human Treg. *Eur. J. Immunol.* **39**, 3315–3322.
13. Tran, D.Q., Andersson, J., Wang, R., Ramsey, H., Unutmaz, D., Shevach, E.M., (2009). GARP (LRRC32) is essential for the surface expression of latent TGF-β on platelets and activated FOXP3+ regulatory T cells. *Proc. Natl. Acad. Sci. USA* **106**, 13445–13450.
14. Harrison, C.A., Al-Musawi, S.L., Walton, K.L., (2011). Prodomains regulate the synthesis, extracellular localisation and activity of TGF-β superfamily ligands. *Growth Factors* **29**, 174–186.
15. Wang, R., Zhu, J., Dong, X., Shi, M., Lu, C., Springer, T.A., (2012). GARP regulates the bioavailability and activation of TGF-β. *Mol. Biol. Cell* **23**, 1129–1139.
16. Qin, Y., Garrison, B.S., Ma, W., Wang, R., Jiang, A., Li, J., et al., (2018). A milieu molecule for TGF-β required for microglia function in the nervous system. *Cell* **174**, (156–71) e16
17. Cui, Y., Hackenmiller, R., Berg, L., Jean, F., Nakayama, T., Thomas, G., et al., (2001). The activity and signaling range of mature BMP-4 is regulated by sequential cleavage at two sites within the prodomain of the precursor. *Genes Dev.* **15**, 2797–2802.
18. Degnin, C., Jean, F., Thomas, G., Christian, J.L., (2004). Cleavages within the prodomain direct intracellular trafficking and degradation of mature bone morphogenetic protein-4. *Mol. Biol. Cell* **15**, 5012–5020.
19. Sopory, S., Kwon, S., Wehrli, M., Christian, J.L., (2010). Regulation of Dpp activity by tissue-specific cleavage of an upstream site within the prodomain. *Dev. Biol.* **346**, 102–112.
20. Akiyama, T., Marques, G., Wharton, K.A., (2012). A large bioactive BMP ligand with distinct signaling properties is produced by alternative proconvertase processing. *Sci. Signal* **5**, ra28.
21. Kunnapuu, J., Tauscher, P.M., Tiusanen, N., Nguyen, M., Loytynoja, A., Arora, K., et al., (2014). Cleavage of the Drosophila screw prodomain is critical for a dynamic BMP morphogen gradient in embryogenesis. *Dev. Biol.* **389**, 149–159.
22. Mi, L.Z., Brown, C.T., Gao, Y., Tian, Y., Le, V.Q., Walz, T., et al., (2015). Structure of bone morphogenetic protein 9 procomplex. *Proc. Natl. Acad. Sci. USA* **112**, 3710–3715.
23. Anderson, E.N., Wharton, K.A., (2017). Alternative cleavage of the bone morphogenetic protein (BMP), Gbb, produces ligands with distinct developmental functions and receptor preferences. *J. Biol. Chem.* **292**, 19160–19178.
24. Gentry, L.E., Webb, N.R., Lim, G.J., Brunner, A.M., Ranchalis, J.E., Twardzik, D.R., et al., (1987). Type 1 transforming growth factor beta: amplified expression and secretion of mature and precursor polypeptides in Chinese hamster ovary cells. *Mol. Cell. Biol.* **7**, 3418–3427.
25. Wakefield, L.M., Smith, D.M., Flanders, K.C., Sporn, M.B., (1988). Latent transforming growth factor-β from human platelets. A high molecular weight complex containing precursor sequences. *J. Biol. Chem.* **263**, 7646–7654.
26. Khalil, N., (1999). TGF-beta: from latent to active. *Microbes Infect.* **1**, 1255–1263.
27. Lee, S.J., McPherron, A.C., (2001). Regulation of myostatin activity and muscle growth. *Proc. Natl. Acad. Sci. USA* **98**, 9306–9311.
28. Thies, R.S., Chen, T., Davies, M.V., Tomkinson, K.N., Pearson, A.A., Shakey, Q.A., et al., (2001). GDF-8 propeptide binds to GDF-8 and antagonizes biological activity by inhibiting GDF-8 receptor binding. *Growth Factors* **18**, 251–259.
29. Hill, J.J., Davies, M.V., Pearson, A.A., Wang, J.H., Hewick, R.M., Wolfman, N.M., et al., (2002). The myostatin propeptide and the follistatin-related gene are inhibitory binding proteins of myostatin in normal serum. *J. Biol. Chem.* **277**, 40735–40741.
30. Zimmers, T.A., Davies, M.V., Koniaris, L.G., Haynes, P., Esquela, A.F., Tomkinson, K.N., et al., (2002). Induction of cachexia in mice by systemically administered myostatin. *Science* **296**, 1486–1488.
31. Simpson, C.M., Stanton, P.G., Walton, K.L., Chan, K.L., Ritter, L.J., Gilchrist, R.B., et al., (2012). Activation of latent human GDF9 by a single residue change (Gly 391 Arg) in the mature domain. *Endocrinology* **153**, 1301–1310.
32. Ge, G., Hopkins, D.R., Ho, W.B., Greenspan, D.S., (2005). GDF11 forms a bone morphogenetic protein 1-activated latent complex that can modulate nerve growth factor-induced differentiation of PC12 cells. *Mol. Cell. Biol.* **25**, 5846–5858.
33. Sengle, G., Ono, R.N., Sasaki, T., Sakai, L.Y., (2011). Prodomains of transforming growth factor β (TGFβ) superfamily members specify different functions:

extracellular matrix interactions and growth factor bioavailability. *J. Biol. Chem.* **286**, 5087–5099.
34. Munger, J.S., Huang, X., Kawakatsu, H., Griffiths, M.J.D., Dalton, S.L., Wu, J., et al., (1999). The integrin αvβ6 binds and activates latent TGFβ1: a mechanism for regulating pulmonary inflammation and fibrosis. *Cell* **96**, 319–328.
35. Mu, D., Cambier, S., Fjellbirkeland, L., Baron, J.L., Munger, J.S., Kawakatsu, H., et al., (2002). The integrin αVβ8 mediates epithelial homeostasis through MT1-MMP-dependent activation of TGF-β1. *J. Cell Biol.* **157**, 493–507.
36. Dong, X., Zhao, B., Iacob, R.E., Zhu, J., Koksal, A.C., Lu, C., et al., (2017). Force interacts with macromolecular structure in activation of TGF-β. *Nature* **542**, 55–59.
37. Wolfman, N.M., McPherron, A.C., Pappano, W.N., Davies, M.V., Song, K., Tomkinson, K.N., et al., (2003). Activation of latent myostatin by the BMP-1/tolloid family of metalloproteinases. *Proc. Natl. Acad. Sci. USA* **100**, 15842–15846.
38. Le, V.Q., Iacob, R.E., Tian, Y., McConaughy, W., Jackson, J., Su, Y., et al., (2018). Tolloid cleavage activates latent GDF8 by priming the pro-complex for dissociation. *EMBO J.* **37**, 384–397.
39. Cotton, T.R., Fischer, G., Wang, X., McCoy, J.C., Czepnik, M., Thompson, T.B., et al., (2018). Structure of the human myostatin precursor and determinants of growth factor latency. *EMBO J.* **37**, 367–383.
40. Shi, M., Zhu, J., Wang, R., Chen, X., Mi, L.Z., Walz, T., et al., (2011). Latent TGF-β structure and activation. *Nature* **474**, 343–349.
41. Wang, X., Fischer, G., Hyvonen, M., (2016). Structure and activation of pro-activin A. *Nat. Commun.* **7**, 12052.
42. Wohl, A.P., Troilo, H., Collins, R.F., Baldock, C., Sengle, G., (2016). Extracellular regulation of bone morphogenetic protein activity by the microfibril component fibrillin-1. *J. Biol. Chem.* **291**, 12732–12746.
43. Fang, J., Nevin, P., Kairys, V., Venclovas, C., Engen, J.R., Beuning, P.J., (2014). Conformational analysis of processivity clamps in solution demonstrates that tertiary structure does not correlate with protein dynamics. *Structure* **22**, 572–581.
44. Wales, T.E., Poe, J.A., Emert-Sedlak, L., Morgan, C.R., Smithgall, T.E., Engen, J.R., (2016). Hydrogen exchange mass spectrometry of related proteins with divergent sequences: a comparative study of HIV-1 nef allelic variants. *J. Am. Soc. Mass Spectrom.* **27**, 1048–1061.
45. Harrison, R.A., Lu, J., Carrasco, M., Hunter, J., Manandhar, A., Gondi, S., et al., (2016). Structural dynamics in Ras and related proteins upon nucleotide switching. *J. Mol. Biol.* **428**, 4723–4735.
46. Wang, J., Su, Y., Iacob, R.E., Engen, J.R., Springer, T.A., (2019). General structural features that regulate integrin affinity revealed by atypical αVβ8. *Nat. Commun.* **10**, 5481.
47. Kochert, B.A., Fleischhacker, A.S., Wales, T.E., Becker, D. F., Engen, J.R., Ragsdale, S.W., (2019). Dynamic and structural differences between heme oxygenase-1 and -2 are due to differences in their C-terminal regions. *J. Biol. Chem.* **294**, 8259–8272.
48. Hinck, A.P., Mueller, T.D., Springer, T.A., (2016). Structural biology and evolution of the TGF-β family. *Cold Spring Harb. Perspect. Biol.* **8**
49. Lienart, S., Merceron, R., Vanderaa, C., Lambert, F., Colau, D., Stockis, J., et al., (2018). Structural basis of latent TGF-β1 presentation and activation by GARP on human regulatory T cells. *Science* **362**, 952–956.
50. Zhao, B., Xu, S., Dong, X., Lu, C., Springer, T.A., (2018). Prodomain-growth factor swapping in the structure of pro-TGF-β1. *J. Biol. Chem.* **293**, 1579–1589.
51. De Sancho, D., Doshi, U., Munoz, V., (2009). Protein folding rates and stability: how much is there beyond size? *J. Am. Chem. Soc.* **131**, 2074–2075.
52. Walton, K.L., Makanji, Y., Chen, J., Wilce, M.C., Chan, K. L., Robertson, D.M., et al., (2010). Two distinct regions of latency-associated peptide coordinate stability of the latent transforming growth factor-beta1 complex. *J. Biol. Chem.* **285**, 17029–17037.
53. Jiang, M.S., Liang, L.F., Wang, S., Ratovitski, T., Holmstrom, J., Barker, C., et al., (2004). Characterization and identification of the inhibitory domain of GDF-8 propeptide. *Biochem. Biophys. Res. Commun.* **315**, 525–531.
54. Ohsawa, Y., Takayama, K., Nishimatsu, S., Okada, T., Fujino, M., Fukai, Y., et al., (2015). The inhibitory core of the myostatin prodomain: its interaction with both type I and II membrane receptors, and potential to treat muscle atrophy. *PLoS ONE* **10**, e0133713
55. Takayama, K., Noguchi, Y., Aoki, S., Takayama, S., Yoshida, M., Asari, T., et al., (2015). Identification of the minimum peptide from mouse myostatin prodomain for human myostatin inhibition. *J. Med. Chem.* **58**, 1544–1549.
56. Takayama, K., Rentier, C., Asari, T., Nakamura, A., Saga, Y., Shimada, T., et al., (2017). Development of potent myostatin inhibitory peptides through hydrophobic residue-directed structural modification. *ACS Med. Chem. Lett.* **8**, 751–756.
57. Chen, J.L., Walton, K.L., Al-Musawi, S.L., Kelly, E.K., Qian, H., La, M., et al., (2015). Development of novel activin-targeted therapeutics. *Mol. Ther.* **23**, 434–444.
58. Walker, R.G., McCoy, J.C., Czepnik, M., Mills, M.J., Hagg, A., Walton, K.L., et al., (2018). Molecular characterization of latent GDF8 reveals mechanisms of activation. *Proc. Natl. Acad. Sci. USA* **115**, E866–E875.
59. Tang, G., Peng, L., Baldwin, P.R., Mann, D.S., Jiang, W., Rees, I., et al., (2007). EMAN2: an extensible image processing suite for electron microscopy. *J. Struct. Biol.* **157**, 38–46.
60. Chen, X., Xie, C., Nishida, N., Li, Z., Walz, T., Springer, T. A., (2010). Requirement of open headpiece conformation for activation of leukocyte integrin alphaXbeta2. *Proc. Natl. Acad. Sci. USA* **107**, 14727–14732.
61. Frank, J., Radermacher, M., Penczek, P., Zhu, J., Li, Y., Ladjadj, M., et al., (1996). SPIDER and WEB: processing and visualization of images in 3D electron microscopy and related fields. *J. Struct. Biol.* **116**, 190–199.
62. Mi, L.Z., Lu, C., Nishida, N., Walz, T., Springer, T.A., (2011). Simultaneous visualization of the extracellular and cytoplasmic domains of the epidermal growth factor receptor. *Nat. Struct. Biol.* **18**, 984–989.
63. Morin, A., Eisenbraun, B., Key, J., Sanschagrin, P.C., Timony, M.A., Ottaviano, M., et al., (2013). Collaboration gets the most out of software. *Elife* **2**, e01456
64. Iacob REB-A, G.M., Makowski, L., Engen, J.R., Berkowitz, S.A., Houde, D., (2013). Investigating monoclonal antibody aggregation using a combination of H/DX-MS and other biophysical measurements. *J. Pharm. Sci.* **102**, 4315–4329.
65. Wales TEF, K.E., Gerhardt, G.C., Engen, J.R., (2008). High-speed and high-resolution UPLC separation at zero degrees Celsius. *Anal. Chem.* **80**, 6815–6820.

66. Masson, G.R., Burke, J.E., Ahn, N.G., Anand, G.S., Borchers, C., Brier, S., et al., (2019). Recommendations for performing, interpreting and reporting hydrogen deuterium exchange mass spectrometry (HDX-MS) experiments. *Nat. Methods* **16**, 595–602.
67. Wales, T.E., Engen, J.R., (2006). Hydrogen exchange mass spectrometry for the analysis of protein dynamics. *Mass Spectrom. Rev.* **25**, 158–170.
68. Perez-Riverol, Y., Csordas, A., Bai, J., Bernal-Llinares, M., Hewapathirana, S., Kundu, D.J., et al., (2019). The PRIDE database and related tools and resources in 2019: improving support for quantification data. *Nucleic Acids Res.* **47**, D442–D450.
69. Krissinel, E., Henrick, K., (2007). Inference of macromolecular assemblies from crystalline state. *J. Mol. Biol.* **372**, 774–797.